Aerosol Science and Technology

ISSN: 0278-6826 (Print) 1521-7388 (Online) Journal homepage: https://www.tandfonline.com/loi/uast20

Application of SERS on the chemical speciation of individual Aitken mode particles after condensational growth

Ryota Kunihisa, Ayumi Iwata, Masao Gen, Chak K. Chan & Atsushi Matsuki

To cite this article: Ryota Kunihisa, Ayumi Iwata, Masao Gen, Chak K. Chan & Atsushi Matsuki (2020) Application of SERS on the chemical speciation of individual Aitken mode particles after condensational growth, Aerosol Science and Technology, 54:7, 826-836, DOI: 10.1080/02786826.2020.1730298

To link to this article: https://doi.org/10.1080/02786826.2020.1730298

AEROSOL SCIENCE AND TECHNOLOGY
2020, VOL. 54, NO. 7, 826–836
https://doi.org/10.1080/02786826.2020.1730298

Application of SERS on the chemical speciation of individual Aitken mode particles after condensational growth

Ryota Kunihisa[a], Ayumi Iwata[b], Masao Gen[c,d], Chak K. Chan[c], and Atsushi Matsuki[e]

[a]Graduate School of Natural Science and Technology, Kanazawa University, Kanazawa, Japan; [b]Faculty of Science and Technology, Keio University, Yokohama, Japan; [c]School of Energy and Environment, City University of Hong Kong, Kowloon Tong, Hong Kong; [d]Faculty of Frontier Engineering, Institute of Science and Engineering, Kanazawa University, Kanazawa, Japan; [e]Institute of Nature and Environmental Technology, Kanazawa University, Kanazawa, Japan

ABSTRACT

The chemical speciation of nanoparticles is technically challenging because of the minute mass of the particles. There is a constant need for more sensitive collection methods and chemical analyses. In this study, we demonstrated the applicability of a surface enhanced Raman scattering (SERS) technique on the rapid and sensitive chemical analysis of individual nanoparticles. SERS technique provides a significant enhancement of the scattering efficiency over traditional Raman spectroscopy. The novelty of the proposed technique is that the SERS substrate is used directly as the sampling substrate of a condensational growth tube (CGT) sampler, which can activate nanoparticles into water droplets and ensure simultaneous inertial sampling and SERS pretreatment. First, we investigated applicability of the method on mono-dispersed (20 nm, 50 nm, or 100 nm) ammonium sulfate (AS) and levoglucosan (LG) particles as model aerosols. The method was then applied to ambient nanoparticles. The successful detection of peaks corresponding to sulfate $\nu(SO_4^{2-})$ and organics ν(C-H) indicates that our proposed method to combine a CGT sampler and SERS showed a sensitivity high enough to provide deep insights into the chemical speciation of atmospheric nanoparticles as small as 20 nm in diameter.

ARTICLE HISTORY
Received 6 November 2019
Accepted 28 January 2020

EDITOR
Jim Smith

Introduction

The size of atmospheric aerosol particles can span over 5 orders of magnitude ranging from a few nm to over 100 µm in diameter. Primary particles from sea spray, desert dust, and biomass burning (Sellegri et al. 2005) are emitted directly into the atmosphere and generally comprise the relatively coarse fraction. Meanwhile, secondary particles are formed from gaseous precursors in the atmosphere by gas-to-particle conversion; these new particles are more often found as nanoparticles in the sub-100 nm diameter range.

The vast majority of secondary particles (by number) in the atmosphere are nanometer scale in diameter, which makes them particularly difficult to control (or remove from the flow) and detect, therefore posing many technical challenges, even today. The minute size and mass of nanoparticles mean that measurements of common physical properties (e.g., light scattering, gravitational sedimentation, and inertia) no longer enable their detection and sizing. Even after a successful classification and collection of size fractionated nanoparticles, the inherently small mass makes it difficult to overcome the detection limits of conventional bulk chemical analyses.

The Spot Sampler (Series 110 Liquid Spot Sample, Aerosol Device Inc.), which is based on condensation growth tube (CGT) technology, can overcome many of the limitations associated with nanoparticle classification and collection (Fernandez, Lewis, and Hering 2014; Lewis and Hering, 2013). In this CGT based sampling system, nanoparticles are magnified through water condensation to form super-micron (~3 µm) droplets, enabling collection, via inertial collectors, of the nanoparticles grown; the droplets are then readily collected into the impaction well and concentrated in a spot ~1 mm (Fernandez, Lewis, and Hering 2014). Efficiencies as high as 98% were reported for dry collection of particles 10 nm to 2.5 µm in size (Fernandez,

CONTACT Atsushi Matsuki matsuki@staff.kanazawa-u.ac.jp Institute of Nature and Environmental Technology, Kanazawa University, Kanazawa 920-1192, Japan.

Supplemental data for this article is available online at https://doi.org/10.1080/02786826.2020.1730298.

Lewis, and Hering 2014). The remaining problem is associated with the rather small throughput (1 liter per minute) of the instrument. It must be coupled with a highly sensitive offline chemical analysis method.

Over the past decade, Raman spectroscopy has been increasingly used for the chemical characterization of atmospheric aerosol particles. Raman spectra are derived from light scattered by samples in an inelastic manner and provide information on molecular vibrational modes (Wang et al. 2015). It has been applied to characterize phase separation (Ciobanu et al. 2009; Yeung and Chan., 2010), ice nucleation properties (Iwata and Matsuki 2018), hygroscopic properties (Ling and Chan., 2008), and the heterogeneous reactivity of atmospheric aerosols (Gen, Huang, and Chan 2018). Specific Raman signals from the fingerprint region (800–1800 cm^{-1}) provide chemical bonding data that are unique to specific molecular structures. Raman spectroscopy has generally been applied on atmospherically relevant particles larger than 1 μm in diameter because of the inherently weak intensity of the Raman scattering signal from fine particles, such that functional groups could not be detected by a spectrometer. However, the vast majority of secondary aerosols in the atmosphere are <1 μm in diameter. Surface-Enhanced Raman Spectroscopy (SERS) can be applied to solve this technical difficulty and detect chemical bonds from nanoparticles.

Fleischmann, Hendra, and McQuillan (1974) first discovered Raman enhancement through the enhanced signal of pyridine on electrochemically roughened silver electrodes. Albrecht and Creighton (1977) and David and Richard (1977) reported SERS as a new phenomenon with the extraordinary enhancement of Raman signals from molecules surrounded by metallic nanostructures. This phenomenon results from highly localized regions, called "hot spots" which occur at gaps between adjacent metal nanostructures (Craig, Bondy, and Ault 2015; Sun et al. 2019). Considerable effort has been focused on the design of an effective and robust SERS active substrate, and other studies applying the SERS technique to atmospheric aerosols used Au inverted pyramids (Fu et al. 2017), electrospray SERS (Gen and Chan 2017; Gen et al. 2019), aerosolized plasmonic colloidosomes (Phan-Quang et al. 2018), and plasmonic bimetallic nanogap structure (Wong et al. 2014) among their tools. Tirella et al. (2018) used Ag foil as an impaction substrate of a microanalysis particle sampler and succeeded in detecting the peaks of inorganic and organic vibrational modes from 150 nm ambient particles. However, this particle size is still larger than the majority of secondary particles in the atmosphere.

In this study, the combination of a differential mobility analyzer (DMA), CGT sampler and the SERS technique is proposed as a new high-efficiency collection and a sensitive analytical method for the chemical speciation of size-resolved particles. It has been tested for its applicability on the chemical speciation of Aitken mode aerosol particles (<100 nm) which are abundant in the atmosphere. The proposed method involves direct collection of nanoparticles onto a SERS substrate following size classification by a DMA and condensational growth by the CGT sampler. The novelty of the coupling of water-based condensation growth technique and the SERS substrate stems from the facts that, 1) the condensing vapor act as pure distilled water that is free of contamination, and 2) because the SERS substrate requires the analyte to be in the form of solution, the condensational growth not only enables inertial collection of nanoparticles, but at the same time serves also as sample pretreatment. These advantages are essential for detecting trace amounts of compounds contained in the nanoparticles.

Materials and methods

Nanoparticle collection on SERS substrate

We selected a commercially available SERS substrate (Ag SERStrate, Silmeco Ltd., Denmark), which has its surface covered by silicon nanopillars coated with silver (Schmidt, Hübner, and Boisen 2012). When the solvent (water) deposited on the substrate evaporates, its surface tension will pull the silicon nanopillars together, trapping the analyte at the hot spots giving rise to a large Raman signal. Hence, using the SERS substrate as an impaction plate of the CGT sampler requires no pretreatment (extraction and dilution) and enables us to directly analyze sample particles later by Raman spectroscopy. In order to grow nanoparticles most efficiently and to dry the collected droplets, the temperature values of conditioner, initiator, moderator, impaction nozzle, and sample plate of the CGT sampler were set at 5 °C, 35 °C, 10 °C, 27 °C, and 32 °C, respectively. The water injection pump added 20 μL of water per 30 sec. Dried spots of sample particles were obtained at a flow rate of 1.0 liter per minute (lpm). Home-made polyethylene terephthalate sample support was prepared to accommodate the SERS substrate (4 × 4 mm dimension) in the collection chamber.

Collection of laboratory-generated nanoparticles

Ammonium sulfate (AS) and levoglucosan (LG) particles were generated in the laboratory as surrogates for atmospherically relevant inorganic and organic

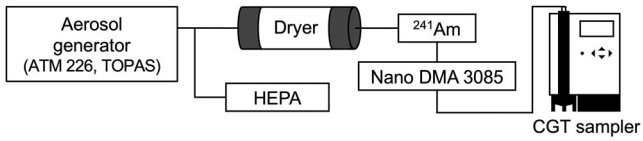

Figure 1. Schematic of the experimental setup used in the laboratory experiment.

aerosols, respectively. Aqueous solutions of AS (Wako Pure Chemical Industries, Ltd.) and LG (Wako Pure Chemical Industries, Ltd.) were prepared at concentrations ranged between 35 ppb (ng/liter) to 1.25 ppm (mg/liter) and 32 ppm to 100 ppm, respectively. Each sample solution was atomized using an aerosol generator (ATM 226. TOPAS, Germany) at a flow rate of 5.0 lpm, with the resulting particle concentrations for both conditions adjusted to 80–90 #/cc. The particles generated were passed through a diffusion dryer to remove water. A neutralizer containing a radioactive source of ^{241}Am was used to provide a known charge distribution on the aerosol entering a DMA. By using a short DMA (Model 3085, TSI Corporation, USA), mono-dispersed particles with electrical mobility diameters of 20 nm, 50 nm, or 100 nm were collected directly on the SERS substrate following condensational growth in the CGT sampler (Figure 1). The sample to sheath flow ratio was set to 1:10 (1 to 10 lpm) for 20 nm and 50 nm particles and 1:5 (1 to 5 lpm) for 100 nm particles to size-select such relatively large particle with the short DMA. Each sampling time was only 1 min.

Collection of ambient nanoparticles

Ambient aerosol samples were collected at the NOTO Ground-based Research Observatory (NOTOGRO, 37.45°N, 137.36°E), Japan (Figure 2) at 15:00 on 2 April, 2019. NOTOGRO is a remote coastal site located on the western coast of central Japan (Ueda et al. 2016; Iwamoto et al. 2016; Schmale et al., 2018; Iwata and Matsuki 2018). Ambient samples were passed through a diffusion dryer before being classified at electrical mobility diameters of 20 nm and 100 nm with an electrostatic classifier (Model 3080, TSI Corporation) equipped with a long DMA (Model 3081, TSI Corporation) at sample-to-sheath flow ratio of 1:10 (1 to 10 lpm) and then collected directly on the SERS substrate using the CGT sampler. Sampling duration was less than 10 min.

Analytical setting for SERS detection

SERS detection was performed using micro-Raman spectroscopy (Nanofinder HE, Tokyo Instruments, Japan). The Raman spectra of individual particles were obtained using a 532 nm excitation laser with the intensity reduced to 0.005 mW by passing through a set of neutral density filters. This is a surprisingly weak laser intensity as compared to the normal Raman analysis, but is required to suppress the background noise at the fingerprint region (1100–1700 cm^{-1}) (Figure S1 in the online supplementary information) that significantly reduces the SERS detection sensitivity (Shan et al. 2017). This background noise is a common characteristic of SERS and popularly known as photocarbonization (Xu et al. 2012), which is considered to be caused by carbon-based surface adsorbates from the atmosphere. With the use of a 100× objective lens (Mitsutoyo, 0.70 N.A.), the laser spot size was estimated to be ~1 μm in diameter. We calibrated both the peak intensity and position in the spectra against the known Raman signal of a pure silicon standard at 520 cm^{-1}. Raman spectra were acquired with an exposure time of 1 s and ten accumulations. Samples were exposed to ambient relative humidity and temperature conditions during Raman analysis (~23 °C and 30 ~ 50% RH).

Results and discussion

Identification of nanoparticles collected on SERS substrate

As mentioned in the methods section, the Ag SERS substrate is comprised of an array of vertically aligned silicon nanopillars coated with Ag. Neighboring nanopillars would lean against each other via surface tension, when the solvent evaporated (Schmidt, Hübner, and Boisen 2012). Therefore, direct collection of magnified nanoparticles by condensational growth on the SERS substrate has additional advantages such that the 1 mm spot deposited by the CGT sampler can easily be identified in optical images. The points where sample droplets are deposited on the surface leave characteristic marks and remains as a trace (Figure 3). The particles grown can be successively impacted and create a 1 mm spot directly beneath the impactor nozzle. In addition, numerous and much smaller 3 μm traces can be observed scattered around the 1 mm spot. This 3 μm size corresponds roughly to the size of a single nanoparticle grown via a water condensation system (Hering, Spielman, and Lewis, 2014). The Spot Sampler is based on the same condensational

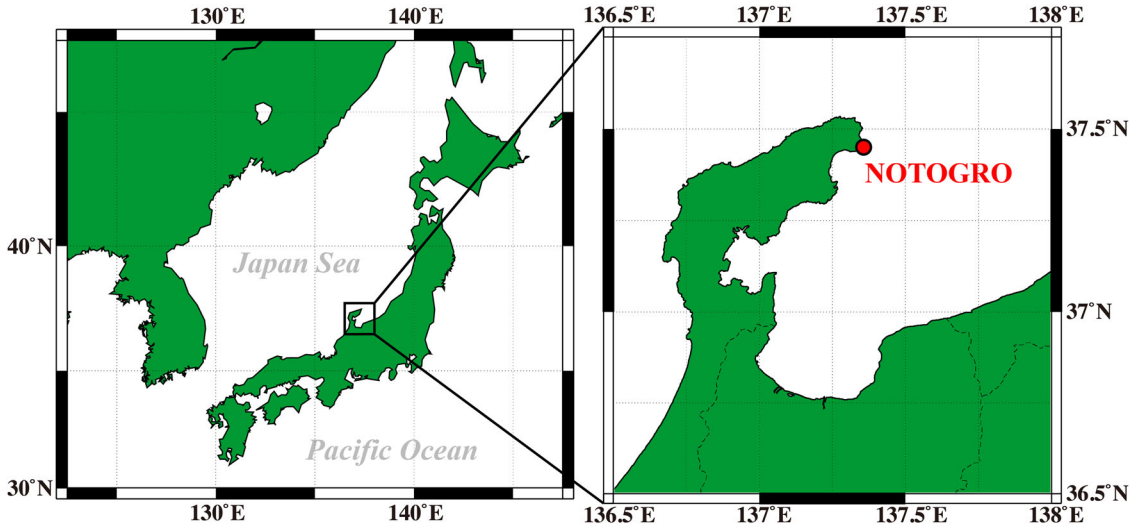

Figure 2. Sampling location of NOTOGRO site.

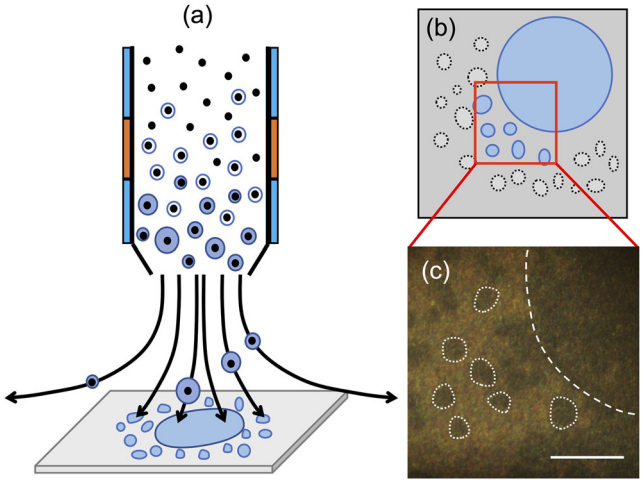

Figure 3. (a) Schematic images of the particle deposition with the CGT sampler. (b, c) Schematic and optical images of the central 1 mm spot and satellite 3 μm traces on the SERS substrate. Scale bar: 10 μm.

growth tube principle of WCPC so that the coagulation of droplets within the tube is unlikely to occur; otherwise WCPC can no longer ensure single particle counting. Therefore, 1 mm spot contains a number of particles, whereas 3 μm trace most likely contains single particle; and to meet our main objective to detect individual particles, we decided to focus Raman laser on the 3 μm traces. We collected in total 30 spectra from laboratory-generated particles, 9 spectra from 20 nm ambient particles and 5 spectra from 100 nm ambient particles. However, the mono-dispersed particle flow by DMA includes particles with multiple charges in the group of those with single charges. Therefore, each trace may not necessarily represent compositions of exactly 20 nm, 50 nm, and 100 nm particles. This limitation also applies to the experiments for ambient particles. Current analysis method does not permit accurate estimation of the multiple charging effect on the overall statistics of collected particles. However, this sort of sizing bias could eventually be resolved e.g., by combining aerosol particle mass (APM) analyzer to extract only the fraction having same mass among the charged particles classified by DMA (Tajima et al. 2011).

Detection of SERS signal from laboratory-generated nanoparticles

AS and LG were selected as surrogates of the atmospherically relevant sulfate and organic particles. AS is well known to be the most abundant atmospheric aerosol component, while LG is the characteristic organic component of particles emitted especially from biomass burning (Hornig et al. 1985; Locker 1988). Laboratory-generated aerosol particles were used to verify if the combination of the CGT sampler

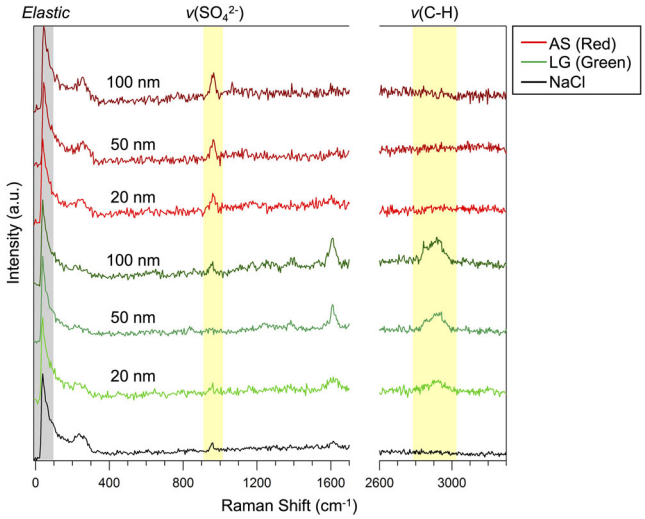

Figure 4. Representative SERS spectra of AS and LG model particles mono-dispersed at 20 nm, 50 nm, and 100 nm. Spectrum of NaCl particle is also shown as a background. Note that spectra for NaCl and LG particles also show a small peak near $\nu(SO_4^{2-})$, which is rather associated with the background (Figure S2).

and the SERS substrate has the capability to detect the Raman scattering from atmospherically relevant nanoparticles.

Raman spectra were acquired from 30 individual 3 μm traces found on the SERS substrate after sampling in respective condition. Representative SERS spectra of model particles are shown separately for 20 nm, 50 nm, and 100 nm in Figure 4. A spectrum of NaCl particle, monodispersed at 50 nm at particle concentration 80–90 #/cc, is included as a reference to confirm if any interfering peaks arise in the background spectra from droplets free of sulfate and organics. Figure 4 shows that all SERS spectra (from LG and AS), as well as NaCl spectra, already had peaks at 40 cm^{-1} and 965 cm^{-1}. The low frequency Raman scattering at 40 cm^{-1} has spontaneously emerged due to the interaction of elastically scattered light and the edge filter (Wei et al. 2018). The latter peak at 965 cm^{-1} is more problematic in this case, since it interferes with the characteristic peak of enhanced sulfate $\nu(SO_4^{2-})$ at ~970 cm^{-1}, which is known to be red-shifted in SERS experiments (Gen and Chan 2017; Fu et al. 2017; Tirella et al. 2018). However, this small peak at 965 cm^{-1} was present even in the case of NaCl or LG samples free of AS, and observed at least on all the SERStrate we tested.

We have looked into the spectra from the substrate itself, and compared with the cases with drops of pure water, ethanol and methanol on the substrate. (Figure S2). The peak at 965 cm^{-1} still remained, but only after deposition of the solvents. From these observations, the possibility of contamination during the water condensation through the CGT system can be excluded. The exact cause of background 965 cm^{-1} peak is not clear, but because of the extreme sensitivity of SERS, molecules from surrounding air may be trapped during the activation of hot spots upon liquid deposition on the substrate and cause this contamination. Further study will be needed to pinpoint the exact source of this background peak in the future.

Despite the presence of the peak at 965 cm^{-1} in the background, the peak intensity of AS particles appears stronger than for LG or NaCl in Figure 4. To verify if the peaks are actually enhanced or not by the presence of additional AS, we normalized the peak intensity at 965 cm^{-1} by that at 40 cm^{-1} (Figure 5a). Wei et al. (2018) reported that the intensity of the surface plasmon enhanced elastic scattering signal (at 40 cm^{-1} in this case) scales linearly with the integrated "hot spot" signals within a laser excitation volume. Thus, intensity of other peaks can be quantified by using the peak intensity at 40 cm^{-1} as a normalizing factor (Wei et al. 2019). In Figure 5a, colored box and whisker plots on the left show the median, average and 95th, 75th, 25th, and 10th percentile values and the right circles show the individual normalized intensity values. The normalized $\nu(SO_4^{2-})$ intensity from AS particles on the SERS substrate was strongly enhanced and consistently larger as compared to the case of NaCl and LG for all particle sizes (20 nm, 50 nm, and 100 nm). Furthermore, the median, average, 75th and 25th percentile values of the normalized $\nu(SO_4^{2-})$ intensity of AS increased with the increasing particle size. This is an indication that the peak intensity increases with the amount of sulfate within the particle (i.e., particle size), and that the current method may even have the potential to semi-quantitatively detect the compound. Note that normal Raman

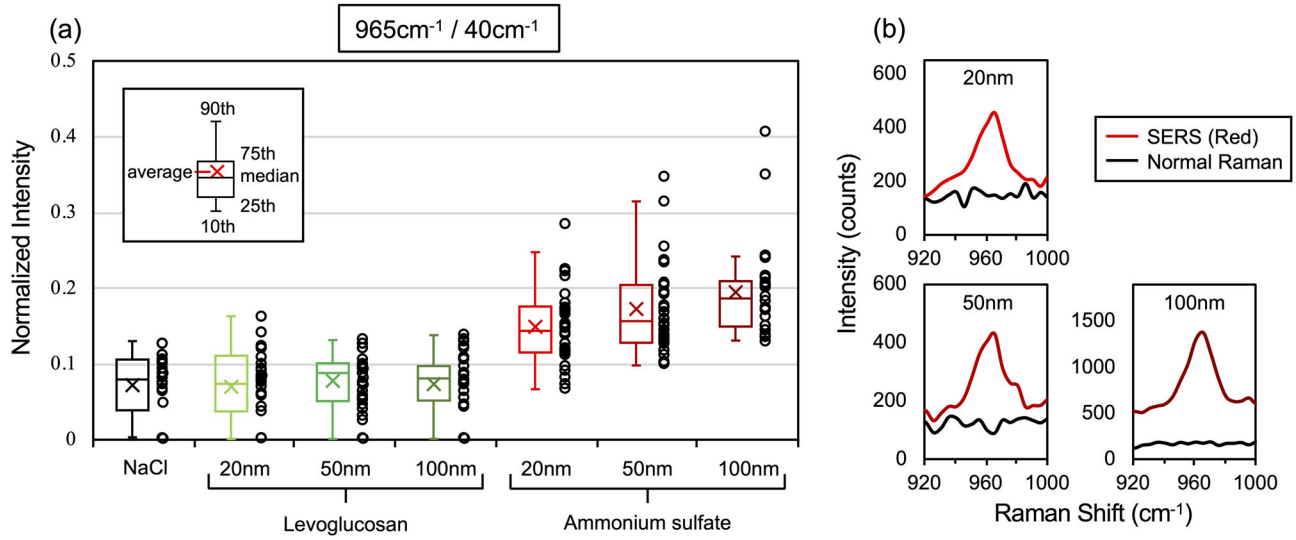

Figure 5. (a) The normalized intensity of the peak at 965 cm^{-1}. Left colored whisker plots showed the median, the average and 95th, 75th, 25th, and 10th percentile values, while the right circles show the individual normalized intensity values. 30 spectra from individual 3 µm traces under each sampling condition were obtained and plotted. (b) SERS and normal Raman spectra for AS 20 nm, 50 nm, and 100 nm particles.

signals were not detected from AS particles collected on a glass substrate (Figure 5b), which is a clear demonstration that detection of such trace amount of compound is only made possible with the aid of the SERS effect of the substrate.

AS should also contain ammonium as the counter cation of sulfate. It is expected to be identified by the peak of ν(N-H) at 3000–3200 cm^{-1} (Venkateswarlu, Bist, and Jain 1975; Dong et al. 2007), however, no noticeable peaks were observed in our spectra. The ν(N-H) mode is a broad peak which results from hydrogen bonding and reported to be weaker than $\nu(SO_4^{2-})$ mode (Degen and Newman, 1993; Jentzsch et al. 2013; Tirella et al. 2018). It is likely that the signal intensity was not strong enough to be detected as a peak in this method, and this may also explain why SERS based detection of ν(N-H) is found only in a limited number of studies. Likewise, the peak of ν(O-H) at 3200–3700 cm^{-1} (Ault et al. 2013) from water was not detected in the spectra. The absence of water peak may partly be related to the fact that the sample plate of the CGT sampler holding the SERS substrate is heated at 32 °C to evaporate water from the droplets during collection (Fernandez, Lewis, and Hering 2014). However, the peak of ν(O-H) cannot be found for LG particles (Figure 4), nor with ethanol and methanol on the SERStrate (Figure S2), suggesting that the signal may be below the detection limit as it was the case for ν(N-H).

Meanwhile, the detection of ν(C-H) region at 2800–3000 cm^{-1} from LG nanoparticles were more straightforward owing to the absence of any interference from background signals and showed strong enhancement even with 20 nm size. Figure 6a shows the normalized peak intensity of the specific peak at 2950 cm^{-1}. Despite the absence of any interfering background peak at 2950 cm^{-1}, we also used the peak intensity at 40 cm^{-1} as a normalization factor to minimize potential point-to-point SERS signal variability. The signal intensity on every spectrum may change depending on the difference on the "hot spot" distribution within a laser excitation volume (Wei et al. 2018). We therefore needed to implement such normalization for comparison. The value from NaCl and AS was virtually 0 because no peaks at 2800–3000 cm^{-1} were found in their spectra. Moreover, the spectra from 100 nm LG particles have an additional peak at 2850 cm^{-1}, corresponding to another ν(C-H) mode (Ault et al. 2013). Similar with AS, the quantitative nature of peak intensity given an increasing particle size was clearly observed. This ν(C-H) mode cannot be detected by normal Raman spectroscopy (Figure 6b).

There is also a characteristic peak found at 1600 cm^{-1} especially with LG particles (Figure 4). This could add to the case for the organic being detected. However, as it was also the case for sulfate at 965 cm^{-1}, a small interfering background peak sometimes appeared even in the case of pure NaCl (though with less intensity as in the case of LG). For this reason, we decided to focus on ν(C-H) stretches around 2800–3000 cm^{-1} for the detection of organics.

Although the individual SERS spectra (the circles in Figures 5a and 6a) originate from mono-dispersed

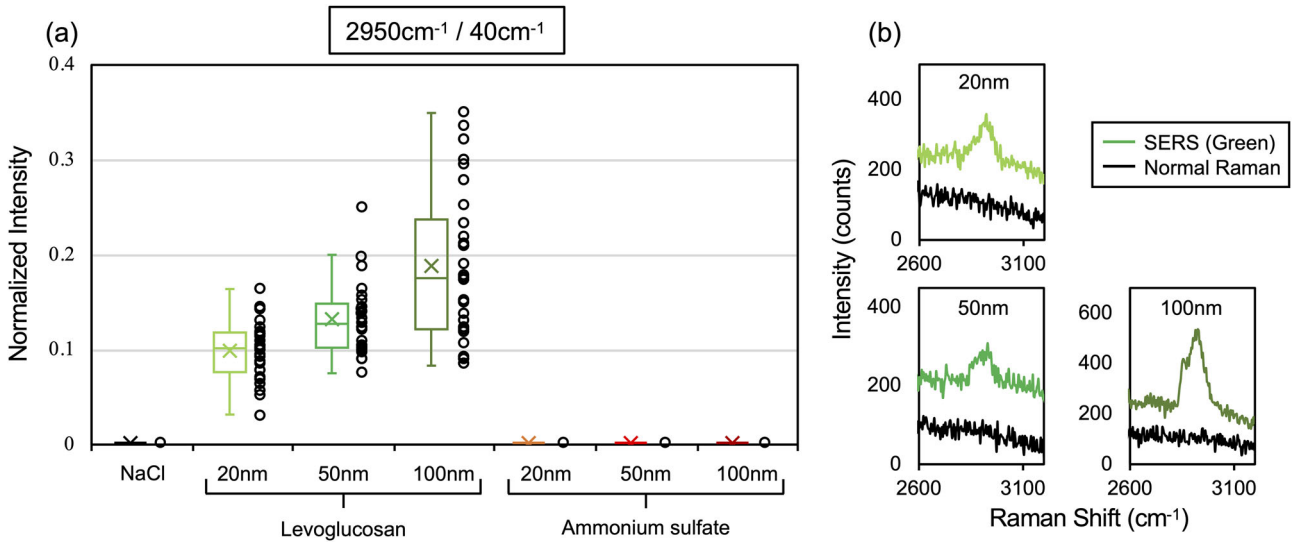

Figure 6. (a) The normalized intensity of the peak at 2950 cm^{-1}. Left colored whisker plots showed the median, the average and 95th, 75th, 25th, and 10th percentile values, while the right colored circles show the individual normalized intensity values. 30 spectra from 3 μm traces under each sampling condition were obtained and plotted. (b) SERS and normal Raman spectra for LG 20 nm, 50 nm, and 100 nm particles.

particles of identical size, they exhibited a wide range of Raman enhancements. In this study, the evaporation of water solvent in a sample droplet deposited onto the SERS substrate allows silver nanopillars to lean against each other and causes them to create a highly localized SERS hot spot. Some analyte molecules adsorbed at the tips of the pillars must be located exactly in the hot spots as the pillars lean together (Schmidt, Hübner, and Boisen 2012). Therefore, it is not necessarily the case that all analyte molecules find their way in the limited hot spots and are enhanced significantly. Schmidt, Hübner, and Boisen (2012) reported that the Raman signal from pre-leaned pillars is approximately 4.5 times lower than from the post-leaned pillars. This situation could also be applied on the Raman signal from analytes that missed the hotspots but instead fell in between the gaps of separated pillars. In addition, the evaporating solution may not leave drying solute homogeneously across the trace, but instead create patches or accumulate selectively along the fringe (in similar manner as the coffee-ring effect). This could partly explain the rather wide spread of the observed Raman enhancements.

These results demonstrated that the combination of the CGT sampler and the SERS substrate has sufficient sensitivity for semi-quantitatively detecting characteristic sulfate and organic signals from individual Aitken mode nanoparticles. Tip-Enhanced Raman Spectroscopy (TERS), which has the advantage of enhanced Raman signal and spatial resolution down to the nanometer scale, has already been applied for nanoparticles smaller than 100 nm in size (Ofner et al. 2016). However, TERS still involves many technical challenges, for example, one must ensure that the excitation laser spot be focused exactly at the probe tip of the scanning probe microscope (SPM) in contact with the analyte. Stable operation of TERS is still not readily achieved and requires highly trained personnel to ensure its reproducibility. In this respect, the proposed method is much quicker, robust and less labor intensive (e.g., does not require additional operation of SPM). Considering the fact that the previous works based on normal Raman and SERS dealt only with accumulation mode particles (>100 nm) or larger (Tirella et al. 2018), the detection of major chemical components from a small volume of nanoparticles as small as 20 nm by SERS can be a significant step forward in our pursuit of developing the more sensitive chemical analysis.

Detection of SERS signal from ambient nanoparticles

We sampled ambient atmospheric nanoparticles mono-dispersed at 20 nm (10-30 #/cc) and 100 nm (100-110 #/cc) at NOTOGRO. The SERS spectra were acquired from the individual 3 μm traces found sparsely on the SERS substrate.

Figures 7a and b show the normalized SERS spectra of ambient 20 nm and 100 nm particles, respectively. Closer look at the peaks of $\nu(SO_4^{2-})$ and ν(C-H) in the SERS spectra of 20 nm ambient particles shows noticeable Raman enhancement at $\nu(SO_4^{2-})$ but not

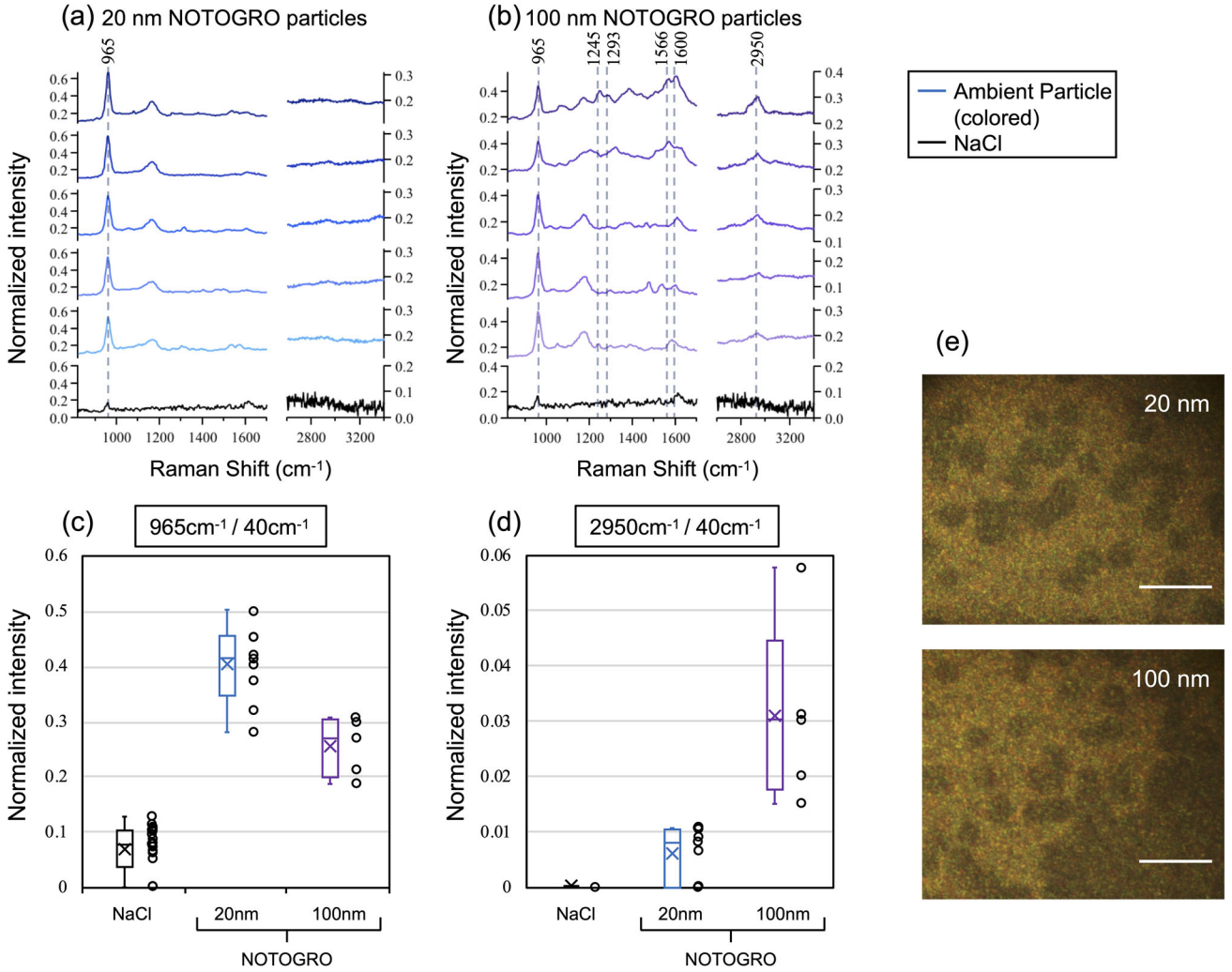

Figure 7. (a, b) Normalized SERS (colored) spectra obtained from ambient particles in NOTOGRO, shown separately for mono-dispersed particles at 20 nm and 100 nm and pure water (black). (c, d) The normalized intensity of the peak at 965 cm^{-1} and 2950 cm^{-1}. Of these spectra, 9 were obtained from 20 nm NOTOGRO ambient particles, while 5 were obtained from 100 nm NOTOGRO ambient particles. Box and whisker plots are shown in the same manner as in Figures 5 and 6. (e) Optical images of 3 μm traces on the SERS substrate under each condition. Scale bars: 10 μm.

as much at ν(C-H) (Figure 7a). Figure 7c shows the normalized intensity of the peak of $\nu(SO_4^{2-})$. While both 20 nm and 100 nm ambient particles showed significantly larger peak intensities as compared to the background (NaCl), the plots for 20 nm were notably higher than those of 100 nm ambient particles. With respect to ν(C-H) on the other hand, Raman enhancement was more pronounced for 100 nm ambient particles (Figures 7b and d), although we still observed weaker enhancement from 20 nm ambient particles. These results imply that sulfate dominates the 20 nm particles rather than the organics, while organics are predominant at 100 nm ambient particle. It may also be worth pointing out that both 20 nm and 100 nm ambient particles were likely in an internal mixing state containing both sulfate and organics but in different mixing ratios.

In addition, there are additional peaks found at the fingerprint region especially for 100 nm ambient particles (Figure 7b). Peaks in the 1100–1700 cm^{-1} region correspond to a range of vibrational modes of organic functional groups. The spectra for 100 nm ambient particles showed enhanced peaks at 1245 cm^{-1}, 1293 cm^{-1}, 1566 cm^{-1}, 1600 cm^{-1}. These peaks may be assigned to the vibration modes of CH_2 and =CH rock, the ring and C=N stretching, and C=C stretching, respectively. It is difficult to identify specific organic components, but this additional data may also provide hints of the kinds of organics present in the ambient nanoparticles. It is also possible that the 1600 cm^{-1} in ambient samples could be due to elemental (graphitic) carbon. However, with the current SERS substrate, it is essential that the analyte molecule be captured exactly at the (sub-nanometer) hotpot in

order to gain enhanced Raman signal. Insoluble particles are generally larger in scale and may have smaller chance of being trapped in the hotpot. Whether the current method can be further extended and demonstrate its applicability also for the insoluble fraction remains a future challenge.

Conclusion

In this study, we proposed that the combined DMA, CGT sampler and SERS techniques can be applied on the chemical speciation of atmospheric nanoparticles by sensitively detecting major chemical components such as sulfate and organics in high time and size resolutions. To the best of our knowledge, this is the first SERS-substrate based study which successfully demonstrated the detection of vibrational modes from Aitken mode (sub-100 nm), individual aerosol particles.

Lab-generated atmospherically relevant particles of AS and LG mono-dispersed at 20 nm, 50 nm, and 100 nm were collected onto the SERS substrate and analyzed with Raman spectroscopy. The SERS spectra showed strongly enhanced peaks of $\nu(SO_4^{2-})$ and ν(C-H) even from particles as small as 20 nm. It is impossible for traditional spectroscopic methods to go down to such sizes due to the extremely small sample mass involved. Moreover, we observed a corresponding increase of the peak intensity with increasing particle size, indicative of semi-quantitative detection. We have demonstrated the compatibility of the CGT sampler and the SERS substrate, through which we were able to overcome some of the major technical challenges associated with collection and measurement of ultrafine particles.

We also found that the combined DMA, CGT sampler and SERS substrate enables identification of characteristic traces on the sampling substrate. The SERS spectra from each of these traces most likely represent the chemical composition of individual nanoparticles. In our initial test on ambient nanoparticles, we observed strongly enhanced peaks of $\nu(SO_4^{2-})$ at 20 nm NOTOGRO ambient particles, while the peak of ν(C-H) was enhanced and detected at 100 nm. Sulfuric acid is believed to be the major contributor to particle growth during the early phases of particle nucleation and growth in the atmosphere; this is likely taken over later, gradually, by organics (Ehn et al., 2014; Meng et al. 2014). Our result may reflect a few snapshots of how chemical species are fractionated among particles of different sizes in the Aitken mode. However, this study is merely a first attempt and more data and careful design of the measurement is needed to draw any definitive conclusion on the chemical dynamics involved in the early stages of the particle growth. Nonetheless, current results showed that the combined CGT sampler and SERS is a promising technique which may provide deeper insights on the chemical speciation of particle growth processes in the atmosphere. We believe that the proposed method makes a significant contribution to the implementation of individual ultrafine particle analysis and could further help solving the aerosol climate uncertainties and health risks related to nanoparticle exposure.

Funding

This study was supported by the Hong Kong Research Grants Council (Grant #11302318), the Japan Society for the Promotion of Science (JSPS) Funding Program for Next Generation World-Leading Researchers (grant no. GR045) and JSPS KAKENHI Grant-in-Aid for Scientific Research B (grant no. JP18H03355).

ORCID

Ayumi Iwata http://orcid.org/0000-0001-6441-2571
Masao Gen http://orcid.org/0000-0001-6160-9029
Chak K. Chan http://orcid.org/0000-0001-9687-8771
Atsushi Matsuki http://orcid.org/0000-0001-7968-414X

References

Albrecht, M. G., and J. A. Creighton. 1977. Anomalously intense Raman spectra of pyridine at a silver electrode. *J. Am. Chem. Soc.* 99 (15):5215–7. doi:10.1021/ja00457a071.

Ault, A. P., D. Zhao, C. J. Ebben, M. J. Tauber, F. M. Geiger, K. A. Prather, and V. H. Grassian. 2013. Raman microspectroscopy and vibrational sum frequency generation spectroscopy as probes of the bulk and surface compositions of size-resolved sea spray aerosol particles. *Phys. Chem. Chem. Phys.* 15 (17):6206–14. doi:10.1039/c3cp43899f.

Ciobanu, V. G., C. Marcolli, U. K. Krieger, U. Weers, and T. Peter. 2009. Liquid – liquid phase separation in mixed organic/inorganic aerosol particles. *J. Phys. Chem. A* 113 (41):10966–78. doi:10.1021/jp905054d.

Craig, R. L., A. L. Bondy, and A. P. Ault. 2015. Surface enhanced raman spectroscopy enables observations of previously undetectable secondary organic aerosol components at the individual particle level. *Anal. Chem.* 87 (15):7510–4. doi:10.1021/acs.analchem.5b01507.

David, L. J., and P. V. D. Richard. 1977. Surface Raman spectroelectrochemistry, part 1: heterocyclic, aromatic, and aliphatic amines adsorbed on the anodized silver electrode. *J. Electroanal. Chem.* 84:1–20. 10.1016/S0022-0728(77.)80224-6.

Degen, I. A., and G. A. Newman. 1993. Raman spectra of inorganic ions. *Spectrochim. Acta. A* 49 (5-6):859–87. doi:10.1016/0584-8539(93)80110-V.

Dong, J. L., X. H. Li, L. J. Zhao, H. S. Xiao, F. Wang, X. Guo, and Y. H. Zhang. 2007. Raman observation of the interactions between NH_4^+, SO_4^{2-}, and H_2O in supersaturated $(NH_4)_2SO_4$ droplets. *J. Phys. Chem. B* 111 (42): 12170–6. doi:10.1021/jp072772o.

Ehn, M., J. A. Thornton, E. Kleist, M. Sipilä, H. Junninen, I. Pullinen, M. Springer, F. Rubach, R. Tillmann, B. Lee, et al, 2014. A large source of low-volatility secondary organic aerosol. *Nature* 506 (7489):476–9. doi:10.1038/nature13032.

Fernandez, A. E., G. S. Lewis, and S. V. Hering. 2014. Design and laboratory evaluation of a sequential spot sampler for time-resolved measurement of airborne particle composition. *Aerosol Sci. Technol.* 48 (6):655–63. doi:10.1080/02786826.2014.911409.

Fleischmann, M., P. J. Hendra, and A. J. McQuillan. 1974. Raman spectra of pyridine absorbed at a silver electrode. *Chem. Phys. Lett.* 26 (2):163–6. doi:10.1016/0009-2614(74)85388-1.

Fu, Y., C. Kuppe, V. K. Valev, H. Fu, L. Zhang, and J. Chen. 2017. Surface-enhanced raman spectroscopy: A facile and rapid method for the chemical component study of individual atmospheric aerosol. *Environ. Sci. Technol.* 51 (11):6260–7. doi:10.1021/acs.est.6b05910.

Gen, M., and C. K. Chan. 2017. Electrospray surface-enhanced Raman spectroscopy (ES-SERS) for probing surface chemical compositions of atmospherically relevant particles. *Atmos. Chem. Phys.* 17 (22):14025–37. doi:10.5194/acp-17-14025-2017.

Gen, M., D. D. Huang, and C. K. Chan. 2018. Reactive uptake of glyoxal by ammonium-containing salt particles as a function of relative humidity. *Environ. Sci. Technol.* 52 (12):6903–11. doi:10.1021/acs.est.8b00606.

Gen, M., R. Kunihisa, A. Matsuki, and C. K. Chan. 2019. Electrospray surface enhanced Raman spectroscopy ES SERS for studying organic coatings of atmospheric aerosol particles. *Aerosol Sci. Technol.* 53 (7):760–70. doi:10.1080/02786826.2019.1597964.

Hering, S. V., S. R. Spielman, and G. L. Lewis. 2014. Moderated, water-based condensational growth of particles in a laminar flow. *Aerosol Sci. Technol.* 48 (4):401–408. doi:10.1080/02786826.2014.881460.

Hornig, J.F., R.H. Soderberg, A.C. BarefootIII, and J.F. Galasyn. 1985. Wood smoke analysis: vaporization losses of PAH from filters and levoglucosan as a distinctive marker for wood smoke. In *Polynuclear aromatic hydrocarbons: Mechanisms, methods, and metabolism*, ed. M. Cooke and A. J. Dennis, 561–8. Columbus: Battelle Press.

Iwamoto, Y., K. Kinouchi, K. Watanabe, N. Yamazaki, and A. Matsuki. 2016. Simultaneous measurement of CCN activity and chemical composition of fine-mode aerosols at noto Peninsula, Japan, in autumn 2012. *Aerosol Air Qual. Res.* 16 (9):2107–18. doi:10.4209/aaqr.2015.09.0545.

Iwata, A., and A. Matsuki. 2018. Characterization of individual ice residual particles by the single droplet freezing method: A case study in the Asian dust outflow region. *Atmos. Chem. Phys.* 18 (3):1785–804. doi:10.5194/acp-18-1785-2018.

Jentzsch, P. V., B. Kampe, V. Ciobota, P. Roesch, and J. Popp. 2013. Inorganic Salts in Atmospheric Particulate Matter: Raman Spectroscopy as an Analytical Tool. *Spectrochim. Acta. A* 115:697–708. doi:10.1016/j.saa.2013.06.085.

Lewis, G. S., and S. V. Hering. 2013. Minimizing concentration effects in water-based, laminar-flow condensation particle counters. *Aerosol Sci. Technol.* 47 (6):645–54. doi:10.1080/02786826.2013.779629.

Ling, T. Y., and C. K. Chan. 2008. Partial crystallization and deliquescence of particles containing ammonium sulfate and dicarboxylic acids. *J. Geophys. Res.* 113 (D14). doi:10.1029/2008JD009779.

Locker, H.B. 1988. The use of levoglucosan to assess the environmental impact of residential wood-burning on air quality. PhD thesis., Dartmouth College, Hanover, NH.

Meng, J. W., M. C. Yeung, Y. J. Li, B. Y. L. Lee, and C. K. Chan. 2014. Size-resolved cloud condensation nuclei (CCN) activity and closure analysis at the HKUST Supersite in Hong Kong. *Atmos. Chem. Phys.* 14 (18): 10267–82. doi:10.5194/acp-14-10267-2014.

Ofner, J., T. Deckert-Gaudig, K. A. Kamilli, A. Held, H. Lohninger, V. Deckert, and B. Lendl. 2016. Tip-enhanced Raman spectroscopy of atmospherically relevant aerosol nanoparticles. *Anal. Chem.* 88 (19):9766–72. doi:10.1021/acs.analchem.6b02760.

Phan-Quang, G. C., H. K. Lee, H. W. Teng, C. S. L. Koh, B. Q. Yim, E. K. M. Tan, W. L. Tok, I. Y. Phang, and X. Y. Ling. 2018. Plasmonic hotspots in air: An omnidirectional three-dimensional platform for stand-off in-air SERS sensing of airborne species. *Angew. Chem. Int. Ed. 57* (20):5792–6. doi:10.1002/anie.201802214.

Schmale, J., S. Henning, S. Decesari, B. Henzing, H. Keskinen, K. Sellegri, J. Ovadnevaite, M. L. Pöhlker, J. Brito, A. Bougiatioti, et al, 2018. Long-term cloud condensation nuclei number concentration, particle number size distribution and chemical composition measurements at regionally representative observatories. *Atmos. Chem. Phys.* 18 (4): 2853–81. doi:10.5194/acp-18-2853-2018.

Schmidt, M. S., J. Hübner, and A. Boisen. 2012. Large area fabrication of leaning silicon nanopillars for surface enhanced Raman spectroscopy. *Adv. Mater.* 24 (10):11–8. doi:10.1002/adma.201103496.

Sellegri, K., Y. J. Yoon, S. G. Jennings, C. D. O'Dowd, L. Pirjola, S. Cautenet, H. Chen, and T. Hoffmann. 2005. Quantification of coastal new ultra-fine particles formation from in situ and chamber measurements during the BIOFLUX campaign. *Environ. Chem.* 2 (4):260–70. doi:10.1071/EN05074.

Shan, F., X.-Y. Zhang, X.-C. Fu, L.-J. Zhang, D. Su, S.-J. Wang, J.-Y. Wu, and T. Zhang. 2017. Investigation of simultaneously existed Raman scattering enhancement and inhibiting fluorescence using surface modified gold nanostars as SERS probes. *Sci. Rep.* 7 (1):6813. doi:10.1038/s41598-017-07311-8.

Sun, Z., F. Duan, K. He, J. Du, L. Yang, H. Li, T. Ma, and S. Yang. 2019. Physicochemical analysis of individual atmosphere fine particles based on effective surface-enhanced Raman spectroscopy. *J. Environ. Sci.* 75:388–95. doi:10.1016/j.jes.2018.06.006.

Tajima, N., N. Fukushima, K. Ehara, and H. Sakurai. 2011. Mass range and optimized operation of the aerosol particle mass analyzer. *Aerosol Sci. Tech.* 45 (2):196–214. doi:10.1080/02786826.2010.530625.

Tirella, P. N., R. L. Craig, D. B. Tubbs, N. E. Olson, Z. Lei, and A. Ault. 2018. Extending surface enhanced Raman spectroscopy (SERS) of atmospheric aerosol particles to the

accumulation mode (150–800 nm). *Environ. Sci.: Process. Impacts* 20 (11):1570–80. doi:10.1039/C8EM00276B.

Ueda, S., T. Nakayama, F. Taketani, K. Adachi, A. Matsuki, Y. Iwamoto, Y. Sadanaga, and Y. Matsumi. 2016. Light absorption and morphological properties of soot-containing aerosols observed at an East Asian outflow site, Noto Peninsula, Japan. *Atmos. Chem. Phys.* 16 (4):2525–41. doi:10.5194/acp-16-2525-2016.

Venkateswarlu, P., H. D. Bist, and Y. S. Jain. 1975. Laser excited Raman spectrum of ammonium sulfate single crystal. *J. Raman Spectrosc.* 3 (2-3):143–51. doi:10.1002/jrs.1250030205.

Wang, W., J. Zhao, M. Short, and H. Zeng. 2015. Real-time in vivo cancer diagnosis using Raman spectroscopy. *J. Biophoton.* 8 (7):527–45. doi:10.1002/jbio.201400026.

Wei, H., W. Leng, J. Song, C. Liu, M. R. Willner, Q. Huang, W. Zhou, and P. J. Vikesland. 2019. Real-time monitoring of ligand exchange kinetics on gold nanoparticle surfaces enabled by hot spot-normalized surface-enhanced Raman scattering. *Environ. Sci. Technol.* 53 (2):575–85. doi:10.1021/acs.est.8b03144.

Wei, H., W. Leng, J. Song, M. R. Willner, L. C. Marr, W. Zhou, and P. J. Vikesland. 2018. Improved Quantitative SERS enabled by surface Plasmon enhanced elastic light scattering. *Anal. Chem.* 90 (5):3227–37. doi:10.1021/acs.analchem.7b04667.

Wong, C. L., U. S. Dinish, K. D. Buddharaju, M. S. Schmidt, and M. Olivo. 2014. Surface-enhanced Raman scattering (SERS)-based volatile organic compounds (VOCs) detection using plasmonic bimetallic nanogap substrate. *Appl. Phys. A* 117 (2):687–92. doi:10.1007/s00339-014-8723-6.

Xu, W., X. Ling, J. Xiao, M. S. Dresselhaus, J. Kong, H. Xu, Z. Liu, and J. Zhang. 2012. Surface enhanced Raman spectroscopy on a flat graphene surface. *PNAS* 109 (24):9281–6. doi:10.1073/pnas.1205478109.

Yeung, M. C., and C. K. Chan. 2010. Water content and phase transitions in particles of inorganic and organic species and their mixtures using micro-Raman spectroscopy. *Aerosol Sci. Technol.* 44 (4):269–80. doi:10.1080/02786820903583786.